Shack–Hartmann centroid detection using the spiral phase transform

J. Vargas,[1,*] R. Restrepo,[2] J. C. Estrada,[3] C. O. S. Sorzano,[1] Yong-Zhao Du,[4] and J. M. Carazo[1]

[1]Biocomputing Unit, Centro Nacional de Biotecnología-CSIC, C/Darwin 3, Cantoblanco, Madrid 28049, Spain

[2]Laboratorio de Instrumentación Espacial, Instituto Nacional de Técnica Aerospacial, Carretera de Ajalvir Km 4, Torrejón de Ardoz, Madrid 28850, Spain

[3]Centro de Investigaciones en Óptica A. C., Loma del Bosque 115, Col. Lomas del Campestre, León, Guanajuato 37150, Mexico

[4]College of Electronic Information, Sichuan University, Chengdu, Sichuan 610064, China

*Corresponding author: jvargas@cnb.csic.es

Received 27 June 2012; accepted 10 September 2012;
posted 19 September 2012 (Doc. ID 171465); published 18 October 2012

We present a Shack–Hartmann (SH) centroid detection algorithm capable to measure in presence of strong noise, background illumination and spot modulating signals, which are typical limiting factors of traditional centroid detection algorithms. The proposed method is based on performing a normalization of the SH pattern using the spiral phase transform method and Fourier filtering. The spot centroids are then obtained using global thresholding and weighted average methods. We have tested the algorithm with simulations and experimental data obtaining satisfactory results. A complete MATLAB package that can reproduce all the results can be downloaded from [http://goo.gl/o2JhD]. © 2012 Optical Society of America

OCIS codes: 100.0100, 120.5050.

1. Introduction

A Shack–Hartmann (SH) wavefront sensor consists on a two-dimensional (2D) microlens array focusing on a CCD camera. The measuring principle of a SH sensor is based on determining the local slopes of an incoming wavefront (W) that is sampled by the microlens array. Each microlens focuses the incident rays into its focal plane where a CCD sensor is placed capturing the spot map, called Hartmann spot diagram. From a high quality reference beam, the displacements $(\Delta x, \Delta y)$ between corresponding centroids of the distorted and reference beams are calculated. Deviation of corresponding spot centroids gives information about the local slopes of the wavefront error (ΔW) [1], that is the difference between the distorted and the reference wavefronts. The 2D field of partial derivatives of the wavefront error is given by [1],

$$\nabla[\Delta W]_{ij} = \left[\begin{pmatrix} \frac{\partial \Delta W}{\partial x} \\ \frac{\partial \Delta W}{\partial y} \end{pmatrix}\right]_{ij} = \left[\frac{1}{f}\begin{pmatrix} \Delta x \\ \Delta y \end{pmatrix}\right]_{ij}, \quad (1)$$

where, ΔW is the wavefront error, f is the distance between the microlens and CCD plane, i, j denotes the ith and jth microlens and $(\Delta x, \Delta y)$ are the displacements between the corresponding distorted and reference spot centroids. We can integrate the wavefront error using the wavefront slope distribution obtained in expression (1), by a zonal or modal reconstruction [2]. We can see from (1) that a crucial step to accurately reconstruct the wavefront error is the

1559-128X/12/307362-06$15.00/0

precise determination of the spot centroids. The accuracy of the centroid detection process is affected by many factors, such as noise (photon noise, detector readout noise), presence of background illumination and spot modulating signals, and sampling and truncation errors, among other problems. The location of the centroid is normally determined calculating the spot center of mass. This method is fast, especially for small numbers of pixels per SH spot, and it is extensively used. However the results obtained from this technique are not accurate in Hartmann patterns affected by noise, background illumination and spot modulating signals. In the past, several approaches have been proposed to accurately obtain the Hartmann centroids in adverse situations such as the weighted centre of gravity (WCOG) [3], the iteratively weighted centroiding [4] and matched filter approaches [5]. In [3] the authors use the centre of gravity method with Gaussian weighting to reduce the influence of pixels situated far from the subaperture center. The Gaussian functions are focused in the pixels corresponding to the center of the subapertures and the full width at half-maximum (FWHM) is predetermined and fixed. This method works very well in noisy SH patterns but it is limited to cases where Δx and Δy are small because of the static character of the Gaussian weighting functions [4]. Therefore, this technique is not appropriate if we are interested in measuring high dynamic range wavefronts. In [4] it is presented an iterative method that improves [3] by making the Gaussian FWHM and the centroid location to be adjusted iteratively. This iterative process allows the algorithm to obtain accurately the centroids in cases where the distorted wavefront is affected by large aberrations, and then the distorted Hartmann spots are not close to the reference ones. These methods can obtain accurate results in presence of noise, but they are not appropriate in cases where the Hartmann pattern is affected by background illumination and spot modulation signals [6]. The matched filter algorithms obtain the shifts that maximize the cross correlation of a reference spot subimage with the problem Hartmann pattern [5,6]. These methods can be used in cases where background light appears but the accuracy is affected by the spot size. For small spots, we can obtain sharp correlation peaks, but on the other hand, in this situation we can obtain false positives when the SH pattern is affected by noise. In the case of having big spots, we will reduce the probability of obtaining false positives in presence of noise, but on the other hand, we will obtain wide correlation peaks so the accuracy will be limited. Additionally, these methods are not adequate in cases where a varying spot modulation or contrast signal appear. In these cases, the magnitude of the correlation peaks varies along the Hartmann pattern.

In this work, we present a centroid detection algorithm capable of measuring in presence of strong noise, background illumination and spot modulating signals in a fast and accurate way. The proposed method is based on the subtraction of the background and the equalization of the modulation signals using the spiral phase transform (SPT) method [7] and Fourier filtering. As a result, we obtain a Hartmann pattern where all the spots have the same maximum intensity, which corresponds to one in arbitrary units (a.u.). Using this preprocessed Hartmann pattern, the spot centroids are obtained using global thresholding and weighted average methods.

In Section 2 we present the proposed method. Section 3 includes some simulations and in Section 4 we show the experimental results. Finally, in Section 5 the conclusions are drawn.

2. Proposed Method

The intensity of a Hartmann spot diagram can be modelled as,

$$I(x,y) = A(x,y) + B(x,y)\cos[\Phi(x,y)] + \eta(x,y), \quad (2)$$

where A is the background illumination term, B is the spot modulating signal, Φ is the spot modulating phase and η is the noise. The background light typically appears because the presence of scattered light as in the aberrometry eye studies, where near infrared light is commonly used. Additionally, the intensity of light beams is commonly not uniform along the aperture; as an example, typically the beam is more intense in points near the beam center than in border points. This effect makes that the spots in a Hartmann pattern usually are affected by a spot modulating or contrast signal (B). If we subtract the background and noise in expression (2) using an isotropic band-pass filter, we have that,

$$\tilde{I} = B\cos[\Phi] = \mathrm{FT}^{-1}[H \cdot \mathrm{FT}[I]], \quad (3)$$

where, $\mathrm{FT}[\cdot]$ and $\mathrm{FT}^{-1}[\cdot]$ denotes the 2D Fourier transform and the 2D inverse Fourier transform, respectively. For the sake of clarity, we have omitted the spatial dependence, and H is an isotropic band-pass frequency filter which is defined as,

$$H = \exp[-(R - R_0)^2/2\sigma^2], \quad (4)$$

where, $R = \sqrt{R_x^2 + R_y^2}$ with R_x and R_y are the frequency components in the Fourier space, R_0 and σ correspond to a rough estimation of the spot frequency and spot frequency standard deviation. In Ref. [7] it is introduced the SPT algorithm and it is shown that this operator transforms a signal into its quasi-quadrature signal as,

$$\mathrm{SPT}[\tilde{I}] = i\exp(iD)B\sin(\Phi), \quad (5)$$

where, D is the direction map and $\mathrm{SPT}[\cdot]$ is the SPT operator that mathematically corresponds to [7],

$$\mathrm{SPT}[\cdot] = \mathrm{FT}^{-1}\left[\left(\frac{R_x + iR_y}{\sqrt{R_x^2 + R_y^2}}\right)\mathrm{FT}[\cdot]\right]. \tag{6}$$

Observe from expressions (5) and (6) that the SPT operator, given in expression (6), transforms $\tilde{I} = B\cos[\Phi]$, into its quasi-quadrature signal that corresponds to $-i\exp(-iD)B\sin[\Phi]$ [7]. Obviously, in order to obtain the quadrature signal of $\tilde{I}$, that is $B\sin[\Phi]$, it is necessary to compute the direction map D. The direction map, defined as the angle that forms the phase gradient with respect to the x-axis, can be obtained from,

$$D = \arctan(\nabla_y \Phi / \nabla_x \Phi). \tag{7}$$

The phase Φ is an unknown quantity and therefore, it is not possible to determine the direction map from (7). Instead of D, we can obtain the orientation map as,

$$\theta = \arctan(\nabla_y \tilde{I} / \nabla_x \tilde{I}). \tag{8}$$

Observe that θ and D are related by the following expression

$$D = \theta + \alpha, \qquad \alpha = \begin{cases} 0 \\ \pi \end{cases}, \tag{9}$$

and then,

$$\exp(iD) = \pm \exp(i\theta). \tag{10}$$

We can see from Expressions (9) and (10) that $\exp(iD)$ and $\exp(i\theta)$ have the same magnitude but possibly different local signs [8].

From expressions (3), (6) and (7) we have that the quadrature signal of $\tilde{I}$ is given by,

$$Q[\tilde{I}] = B\sin(\Phi) = -i\exp(-iD)\mathrm{SPT}[\tilde{I}], \tag{11}$$

where $Q[\cdot]$ corresponds to the quadrature operator. We can obtain the quasi-quadrature operator, that will be affected by local sign ambiguity [8] as

$$\hat{Q}[\tilde{I}] = -i\exp(-i\theta)\mathrm{SPT}[\tilde{I}]. \tag{12}$$

From Expressions (3) and (12), we can obtain the modulating phase Φ at every pixel, and affected by the local sign ambiguity as,

$$\Phi(x,y) = \pm\arctan\left[\frac{\hat{Q}[\tilde{I}(x,y)]}{\tilde{I}(x,y)}\right]. \tag{13}$$

We compute the normalized version of I, that corresponds to $A = 0$ and $B = 1$ at every pixel position in Expression (1) as,

$$I_n = \cos[\Phi(x,y)] = \cos\left[\arctan\left[\frac{\hat{Q}[\tilde{I}]}{\tilde{I}}\right]\right]. \tag{14}$$

Note that the cosine is an even function so it will not be affected by the local sign ambiguity in $\exp(i\theta)$. The modulating signal $\tilde{B}$ after applying the band-pass filter H is given by,

$$\tilde{B} = \sqrt{\hat{Q}[\tilde{I}]^2 + \tilde{I}^2}. \tag{15}$$

Once obtained I_n, we can easily segment the pattern with a global threshold typically around an intensity value of 0.2 (a.u.). Finally, each spot centroid is extracted by a weighted average using as weights the spots intensity in I_n and the modulating signal $\tilde{B}$, that can be interpreted as a quality map [9], as,

$$\begin{aligned} x_c &= \sum_{x,y} x I_n \tilde{B} \Big/ \sum_{x,y} I_n \tilde{B} \\ y_c &= \sum_{x,y} y I_n \tilde{B} \Big/ \sum_{x,y} I_n \tilde{B}. \end{aligned} \tag{16}$$

3. Simulations

In order to show the effectiveness of the proposed method, we have performed some simulations. We have compared the results obtained by the proposed method (SPT) with the results acquired by the WCOG [3] and iterative weighted centre of gravity (IWCOG) [4] approaches. In Figs. 1(a), we show a simulated Hartmann pattern affected by noise, background and modulation signals. The noise is Gaussian and additive with a signal-to-noise-ratio (SNR) of 6.25%. The Hartmann diagram has size of 300 × 300 px and contains 400 spots. The background and modulation signals correspond to $A = x/5 \cdot 10^3$ and $B = \exp[-0.9(x^2 + y^2)/2 \cdot 10^4]$ both in (a.u.). The wavefront error (ΔW) and its derivatives in the x and y axis are shown in Fig. 2(a), 2(b) and 2(c) respectively. Observe that the dynamic range of the wavefront error is of 117 (a.u.). In Fig. 1(b) we show the recovered normalized SH pattern and the obtained centroids. Finally, in Fig. 1(c) we present the computed modulation map, $\tilde{B}$, used in the weighted average. The root-mean-square error (rms) between the recovered and the ground truth centroids is of 0.31, 0.37, and 0.31 px when are used the SPT, WCOG, and IWCOG, respectively. Note that the results acquired by the IWCOG method have been obtained after four iterations. Additionally, the respective processing times are 0.8, 2.7 and 19.2 s when processing with MATLAB and using a 2.67 GHz laptop. In Fig. 3, we show the differences between the ground truth and obtained centroids in the x and y axis. As can be seen from Fig. 3, the centroid error diagrams are centered at pixel (0, 0) in all cases, so there is no a systematic error in the different centroid extraction algorithms. As can be seen from the results above, the proposed algorithm

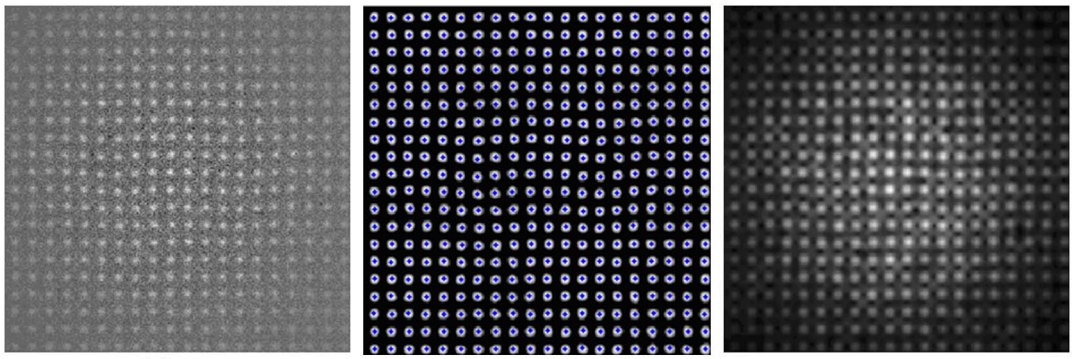

Fig. 1. (Color online) (a) Simulated Hartmann pattern affected by noise, background and modulation signals, (b) recovered normalized SH pattern and the obtained centroids, and (c) computed modulation map $\tilde{B}$.

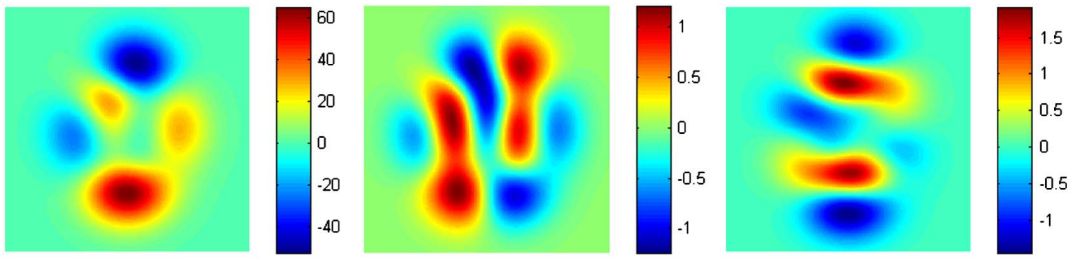

Fig. 2. (Color online) (a) Simulated wavefront error (ΔW), (b) its derivatives in the x axis, and (c) y axis, respectively.

retrieves the SH centroids in a faster way than the WCOG and IWCOG approaches (approximately 3.4 and 24 times faster respectively) but with accuracy similar to the IWCOG method.

We have also studied the accuracy of the different algorithms for different noise levels, spot sizes and wavefront error dynamic ranges. In all cases, we have used the same background and modulation terms than in Fig. 1(a). In Fig. 4 we show the obtained results, where the gray line with circles, the red line with triangles and the blue line with squares denote the results obtained by SPT, the WCOG and IWCOG methods, respectively. All the results acquired by the IWCOG method have been obtained after four iterations. In Figs. 4(a) and 4(d) we analyze the accuracy of the different methods for different levels of noise and using two different wavefront dynamic ranges, since in Figs. 4(b) and 4(c) we study the influence of the Hartmann spot size and wavefront dynamic range in the retrieved accuracy. Note that in Figs. 4(b) and 4(c) we have used a SNR of 1%, in Figs. 4(a) and 4(c) a spot size of 8 px and in Figs. 4(a) and 4(b) a wavefront dynamic range of 117 (a.u.), as was used in the first simulation. Finally, in Fig. 4(d) we use a wavefront dynamic range of 176 (a.u.). Note, that the results shown in Figs. 4(a) and 4(d) are obtained using the same parameters except the wavefront dynamic range. We have repeated this numerical experiment in order to explain the good performance of the WCOG method for high levels

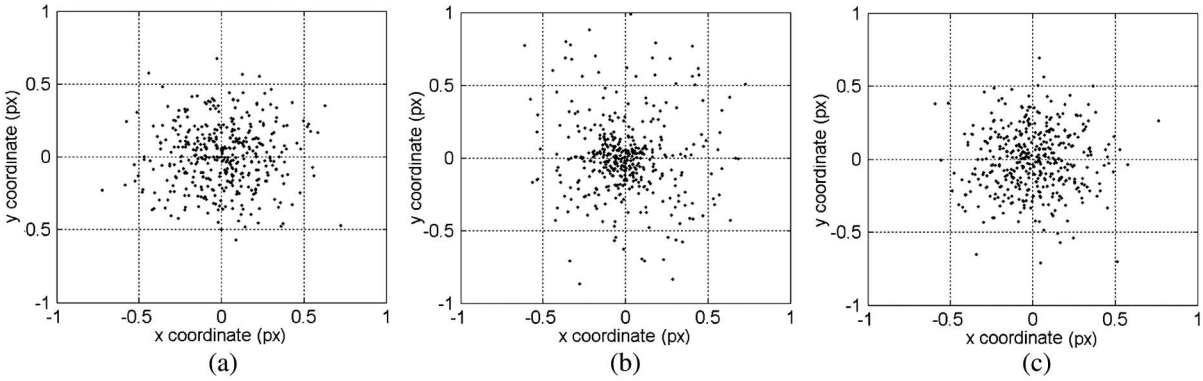

Fig. 3. Difference between the ground truth and obtained centroids in the x and y axis when it is used with the proposed (a) SPT, (b) WCOG, and (c) ICOG approaches.

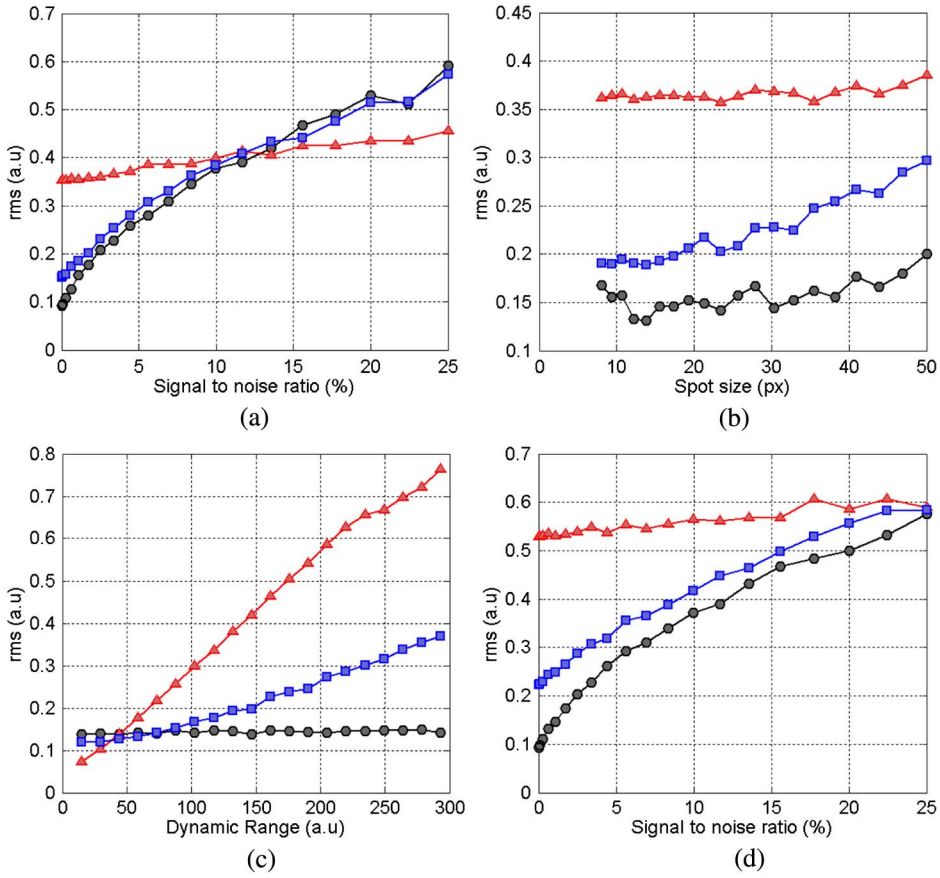

Fig. 4. (Color online) (a) Root-mean-square error versus noise level, (b) spot size, and (c) wavefront error dynamic ranges for the different methods.

of noise shown in Fig. 4(a). As can be seen in Fig. 4(d), this good behavior does not appear when we increase the wavefront dynamic range. Therefore the good results presented in Fig. 4(a) for high levels of noise are because the reference and distorted centroids and very close for the wavefront dynamic range used in this simulation. Additionally, from Figs. 4(b) and 4(c) we can see that there is a no significant dependence between the accuracy, the spot size and the wavefront dynamic range when we use the proposed method, but this is not the case when it is used the IWCOG and WCOG approaches.

4. Experimental Results

We have also tested the proposed algorithm with an experimental SH pattern obtained in an aberrometry eye study that it is shown in Fig. 5(a). Observe from Fig. 5(a) that the pattern is affected by background illumination, spot modulating signals and strong noise. In Fig. 5(b) we show the recovered normalized SH pattern and the obtained centroids. Finally, in Fig. 5(c) we show $\tilde{B}$ map. The processing time is of 1.1 s and the SH pattern size of 337 × 334 px.

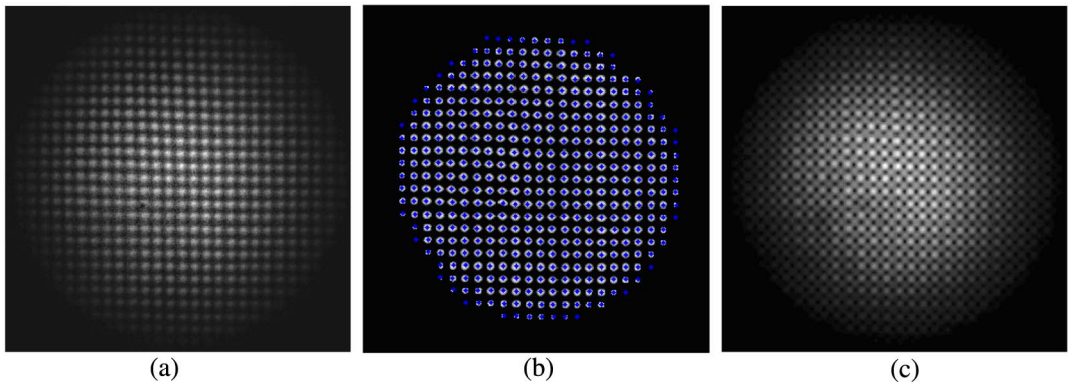

Fig. 5. (Color online) (a) Real Hartmann pattern, (b) recovered normalized pattern and obtained centroids, and (c) $\tilde{B}$ map.

5. Conclusions

In conclusion, we have presented a straightforward, accurate and fast SH centroid detection algorithm. This approach is capable to measure in presence of strong noise, background illumination and spot modulating signals; that are the typical limiting factors of the traditional centroid detection algorithms. The proposed method is based on the SPT method and Fourier filtering. We have tested the algorithm with simulations and experimental data and we have compared the behavior of the proposed algorithm with the WCOG approach [3] and the IWCOG method [4] obtaining satisfactory results where we have show that the proposed approach is 3.4 and 24 times faster respectively than the WCOG and IWCOG methods and more accurate. A complete MATLAB package that can reproduce all the results can be downloaded from [10].

The authors would like to acknowledge economic support from the Spanish Ministry of Economy and Competitiveness through grants ACI2009-1022, ACI2010-108 and BIO2010-16566 and postdoctoral "Juan de la Cierva" grant with reference JCI-2011-10185. C. O. S. Sorzano is recipient of a Ramón y Cajal fellowship.

References

1. R. G. Lane and M. Tallon, "Wave-front reconstruction using a Shack–Hartmann sensor," Appl. Opt. **31**, 6902–6908 (1992).
2. D. N. Neal, J. Copland, and D. Neal, "Shack–Hartmann wavefront sensor precision and accuracy," Proc. SPIE **4779**, 148–160 (2002).
3. M. Nicolle, T. Fusco, G. Rousset, and V. Michau, "Improvement of Shack–Hartmann wavefront sensor measurement for extreme adaptive optics," Opt. Lett. **29**, 2743–2745 (2004).
4. K. L. Baker and M. M. Moallem, "Iteratively weighted centroiding for Shack–Hartmann wavefront sensors," Opt. Express **15**, 5147–5159 (2007).
5. L. A. Poyneer, D. W. Palmer, K. N. LaFortune, and B. Bauman, "Experimental results for correlation-based wavefront sensing," Proc. SPIE **5894**, 58940N (2005).
6. C. Leroux and C. Dainty, "Estimation of centroid positions with a matched-filter algorithm: relevance for aberrometry of the eye," Opt. Express **18**, 1197–1206 (2010).
7. K. G. Larkin, D. J. Bone, and M. A. Oldfield, "Natural demodulation of two-dimensional fringe patterns. I. General background of the spiral phase quadrature transform," J. Opt. Soc. Am. A **18**, 1862–1870 (2001).
8. J. Villa, I. De la Rosa, G. Miramontes, and J. A. Quiroga, "Phase recovery from a single fringe pattern using an orientational vector-field-regularized estimator," J. Opt. Soc. Am. A **22**, 2766–2773 (2005).
9. B. Strobel, "Processing of interferometric phase maps as complex-valued phasor images," Appl. Opt. **35**, 2192–2198 (1996).
10. http://goo.gl/o2JhD.